ELSEVIER

Ceramics International 25 (1999) 125–135

CERAMICS INTERNATIONAL

Crystallisation and sintering behaviour of nanocrystalline Y-TZP powders obtained by seeding-assisted chemical coprecipitation

P. Durán*, J. Tartaj, J.F. Fernández, M. Villegas, C. Moure

Instituto de Cerámica y Vidrio (CSIC), Electroceramics Department, 28500-Arganda del Ray, Madrid, Spain

Received 10 September 1997; accepted 20 October 1997

Abstract

Addition of nanometric-size Y-TZP seed particles to yttrium–zirconium cation sols resulted in a lowering (50 to 100°C) of the air-crystallisation temperature of the Y-TZP (3 mol% Y_2O_3) phase, and a strong increase in the crystallisation rate (about one order of magnitude higher) for the formation of Y-TZP phase in air-calcined coprecipitated amorphous powders relative to the unseeded Y-TZP ones. The isothermal crystallisation rates for the Y-TZP formation in unseeded and polycrystalline Y-TZP seeded (10 wt%) Y-TZP amorphous precursors were well fitted by an Avrami-type kinetic relationship. Addition of nanometric-size Y-TZP seed particles to Y-TZP amorphous precursors reduced the apparent activation energy for the Y-TZP crystallisation process from 184 to 119 kJ mol^{-1}. Fully transformed seeded Y-TZP coprecipitated amorphous precursors (375°C for 10 h) retained $\geq 100\ m^2\ g^{-1}$ surface area, and exhibited a mainly mesoporous structure with relatively narrow pore size distributions. Green compacts of such a Y-TZP powders sintered at near theoretical density at a temperature as low as 1050°C for 5 h with a grain size within the nanoscale (< 100 nm).

Keywords: A. Sintering; Tetragonal zirconia; Crystallization; Seeding

1. Introduction

It is widely recognised that ceramic materials having an ultrafine grain size, i.e., nanostructured, present unusual mechanical, electrical, and magnetic properties. Owing to its high strength and toughness, yttria-doped tetragonal zirconia polycrystals (Y-TZP) is one of the most interesting ceramic materials for structural applications [1–3]. Besides this, when the grain size is submicronic Y-TZP ceramics show a superplastic behaviour at elevated temperatures [4–6]. This being so, the superplastic forming could be used for the fabrication of complex shape Y-TZP components with controlled dimensionality. To evaluate those properties it is necessary the availability of ceramic materials having both near theoretical density and a grain size within the nanoscale (< 100 nm). To achieve ceramic materials with these two characteristics is only possible by free-sintering at lower temperatures than those currently used or by pressure-assisted sintering [7–9]. At any case the use of powders with high sinterability and good compactability become necessaries. Those powder characteristics are closely related to the strength of the interparticles bonds. Such a strength can be decreased by lowering the Y-TZP crystallisation temperature. The lower is the crystallisation temperature the lower is the strength of the interparticles bonds.

It is commonly accepted that chemical methods lead to powders with no compositional fluctuations and controlled size and shape [10,11]. However in most of them metastable compounds are obtained needing a subsequent calcination step (500°C) to convert the gels in an oxidic ceramic powder. In the last decade, the hydrothermal synthesis route has been successfully used in the preparation of many ultrafine ceramic powders [12–14]. This technique although do not needs the calcination step to obtain oxides but involves the use of a closed vessel operating at relatively high temperatures (200 to 350°C) and pressures (~100 bars). Besides this a further heat treatment at about 300°C become necessary to eliminate residual organic or inorganic products before using the ceramic powders. On the other hand parameters like pH, concentration, and liquid medium have to be carefully adjusted to obtain sinterable powders with controlled morphology. It is for these reasons

* Corresponding author. Fax: +34-1-870 0550.

0272-8842/99/$—see front matter
PII: S0272-8842(98)00012-1

that such a chemical route of synthesis has not attracted the attention which has been paid to sol–gel or coprecipitation processing as the main routes to advanced ceramic powders.

Recently, the technique of inert-gas condensation combined with in situ powder compaction is being used for the preparation of nanostructured pure ZrO_2 powders [15–17]. The process consists of evaporation of zirconia monoxide in an inert-gas atmosphere of 250 to 1500 Pa followed by a post-oxidation step of the small ZrO-crystals accumulated on the surface of a cold finger kept at 77 K. In order to avoid agglomeration of the highly reactive ZrO nanoparticles the post-oxidation step is carried out at a controlled rate, and a stoichiometric ZrO_2 is obtained by annealing the as prepared powders at 300°C in an oxygen atmosphere. Such a technique, as reported by Skandan et al. [18], could not be used for the preparation of nanostructured Y-TZP powders. Other physical methods, such as laser ablation [19] and high energy ball milling [20] are also being explored to synthesize nanosized powders.

From all the above described powder preparation methods, because of its easiness and low cost, is the chemical coprecipitation the preferred one to produce massively nanocrystalline powders in spite of the relatively high calcination temperature used, 500 to 600°C in the specific case of the Y-TZP powders, and the relatively strong interparticles bonds formed during such a heat-treatment.

Given that the crystallisation temperature is a key parameter controlling the strength of the interparticles bonds, the claim of this study is the use, to our best knowledge for the first time in the case of the Y-TZP, of the "seeding fundamental concepts" successfully applied in the case of the Al_2O_3 and Al_2O_3–SiO_2 systems [21–24], to lowering the crystallisation temperature and/or modifying the crystallisation kinetics of air-calcined Y-TZP amorphous precursors. The approach adopted involved the incorporation of Y-TZP nanometer-size seed particles into the Y-TZP amorphous matrix. On the other hand, the characteristics of the Y-TZP powders so obtained and their sintering behaviour will also be studied. The results will be compared with that of a commercial (Tosoh) Y-TZP powder.

2. Experimental procedure

The details of the seeded Y-TZP amorphous powders preparation have been described elsewhere [25]. Briefly, we prepare Y-TZP amorphous precursors by dissolving $Zr(C_4H_9O)_4.C_4H_9OH$ and $Y(NO_3)_3.6H_2O$ in pure 2-propanol slightly acidulated with HNO_3. This sol-solution was labelled as A. A portion of this sol-solution was added to a mixture of 2-propanol + NH_4O_H by stirring up to complete coprecipitation of the Zr^{4+} and Y^{3+} hydroxides. After filtering and thoroughly washing with pure 2-propanol,the precipitate was calcined at 450°C for 5 h to obtain the Y-TZP seed particles (~8 nm) as determined from the analysis of X-ray line broadening, using the Sherrer formula. A suspension in pure 2-propanol containing 10 wt% Y-TZP seed nanoparticles in proportion to the final Y-TZP oxide product, was prepared. This Y-TZP suspension was labelled as B. Then the sol-solution A and suspension B were mixed by powerful agitation for 1 h to ensure a homogeneous dispersion of the Y-TZP nanoparticles. By adding a mixture of pure 2-propanol + NH_4OH to the above dispersion by stirring, a complete coprecipitation was obtained after 2 h maintaining a pH≥9 during all the process. After washing, with pure 2-propanol for four or five times and drying in an oven overnight at 80°C, a loose powder of Y-TZP amorphous precursor containing the Y-TZP seed nanoparticles was obtained. This powder preparation process was named as seeding-assisted chemical coprecipitation (SACC). For comparisons an unseeded Y-TZP amorphous precursor powder prepared in the same way was used.

For isothermal kinetic measurements a known amount of the unseeded and seeded Y-TZP amorphous powders were heated in a small platinum crucible for soaking times which varied from 0.1 to 60 h in an isothermal mode in the temperature range of 320 to 400°C. After heating, the amounts of crystallised tetragonal phase was measured by quantitative XRD (Siemens D 5000 with Cu radiation) on the 111 peak area using a previously calibrated curve. A differential thermal analyzer (DTA/TG, Netzsch STA-409) was also used to study the onset, maximum, and the end temperatures of the crystallisation process. The heating rate was in all the cases of 5°C min.$^{-1}$ Specific surface areas of the Y-TZP powders were calculated by the BET method (Accusorb 210 E, Micromeritis), and the crystallite size D_{111} of the calcined powders was measured for the (111) reflection by X-ray line broadening using the Scherrer formula [26]; $D_{111} = 0.94\lambda/B_{111}\cos\theta$, where B_{111} is the half width of the peak duly corrected for the effect of the spectral and the instrumental broadening. Powder morphology was observed by scanning electron microscopy (SEM, Zeis DSM 950) and transmission electron microscopy (TEM, Jeol 2000 FX).

Sintering experiments were carried out on seeded Y-TZP powders calcined at 375°C for 10 h. After compaction at 200 Pa, pore size distributions in green compacts were obtained using mercury porosimetry (Autopore II, 9215). The green compacts were then heated in non-isothermal conditions up to 1400°C at 5°C min^{-1}. Sintered densities were measured by the Archimedes method with distilled water. Microstructure development was observed by SEM on both polished and fractured thermally etched surfaces. Grain size was measured on the SEM micrographs by the interception method [27].

3. Results and discussion

3.1. Crystallisation characteristics

Fig. 1 shows the results of the differential thermal analysis of the seeded Y-TZP amorphous precursors comparatively with those of the pure hydrous zirconia and unseeded Y-TZP powders. The exothermic peak represents the crystallisation temperature for pure zirconia tetragonal and yttria-doped tetragonal zirconia, respectively. The crystallisation temperature of tetragonal zirconia increases with the addition of Y_2O_3 from about 420 to 455°C for the unseeded Y-TZP amorphous precursors, and diminished up to about 418°C for the seeded Y-TZP ones. The asymmetry of the exothermic peak increased from the pure hydrous zirconia to the seeded Y-TZP amorphous precursors, which is indicating a certain heat releases associated, probably, with the enthalpy of the tetragonal solid solution formation. Such heat release start to be detected at about 418 and 310°C for unseeded and seeded Y-TZP amorphous precursors, respectively. This means that the yttria-doped tetragonal zirconia solid solution crystallisation starts at a temperature, at least, 100°C lower in the seeded Y-TZP amorphous precursors. Being this so, then a completely crystallised tetragonal zirconia phase could be obtained by calcining in air seeded Y-TZP amorphous precursors in the temperature range of 310 to 418°C. In fact, the seeded Y-T7P amorphous precursors calcined at 320°C for 20 h was about 80% crystallised tetragonal zirconia phase (without traces of other phases), whereas the unseeded Y-TZP amorphous precursors remained amorphous at the same temperature even after an annealing of 40 h (Fig. 2). Livage et al. [28] established that pure zirconia could start to crystallise at 300°C, and a minimum temperature of 350°C would required for complete crystallisation. Theunissen et al. [29] observed the onset of crystallisation for Y-TZP at 400°C and Boutz et al. [30] established by DSC experiments the amorphous to crystalline transition for Y-TZP at 450°C. According to our surprising results both the decrease in the onset of the crystallisation temperature and the increase of the Y-TZP crystallisation rate could be attributed, in principle, to a lower activation energy required to nucleate the Y-TZP phase from the seeds. If as suggested by Livage et al. [28] the crystallisation of pure tetragonal zirconia from amorphous powders started by nucleation at favoured points then it should be assumed that an increasing of the nucleation density sites would shift the onset of the crystallisation to lower temperatures. Figs. 3(a) and (b) show XRD patterns for unseeded and seeded Y-TZP amorphous precursors which were calcined at temperatures in the range of 350 to 400°C for 0.5 to 1 h. As it can be observed the unseeded samples remained amorphous at 350 and 375°C and no more than 30% of crystallised tetragonal phase was obtained at 400°C. The relative amount of this phase was strongly increased in 10 wt% seeded Y-TZP sample. As Y-TZP seeds were homogeneously distributed, they promoted heterogeneous nucleation of tetragonal phase. The rapid crystallisation of the newly formed tetragonal phase was, favoured probably, because of epitaxial growth on the surface of the homogeneously distributed isostructural crystalline Y-TZP seed nanoparticles. Thus, nanocrystalline seeded Y-TZP amorphous precursors crystallised epitaxially to tetragonal phase at 350°C and below, (Fig. 2) while the unseeded Y-TZP precursors were amorphous even at 375°C. The very small particle size of the Y-TZP seeds (~8 nm) did not show detectable changes in the XRD intensities, but the epitaxial crystallisation has also been evidenced in many other seeded-gels to ceramic

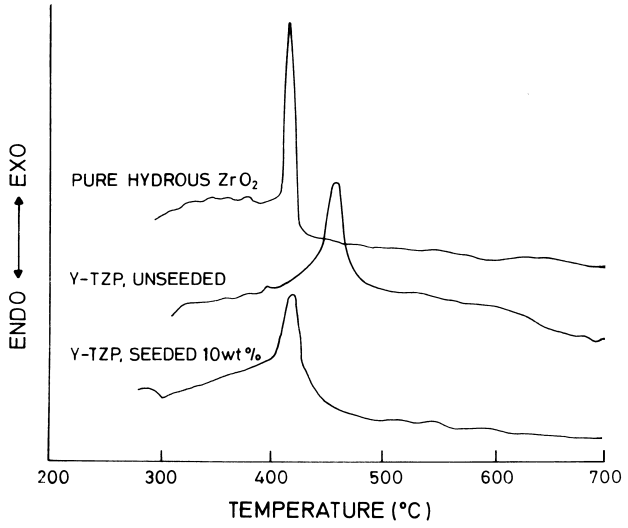

Fig. 1. DTA heating curves for pure hydrous zirconia, unseeded, and 10 wt% seeded Y-TZP amorphous precursors.

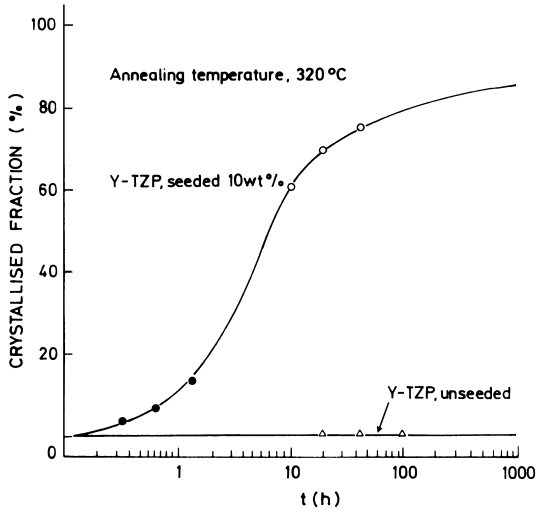

Fig. 2. Crystallisation of unseeded and 10 wt% seeded Y-TZP amorphous precursors as a function of time duration.

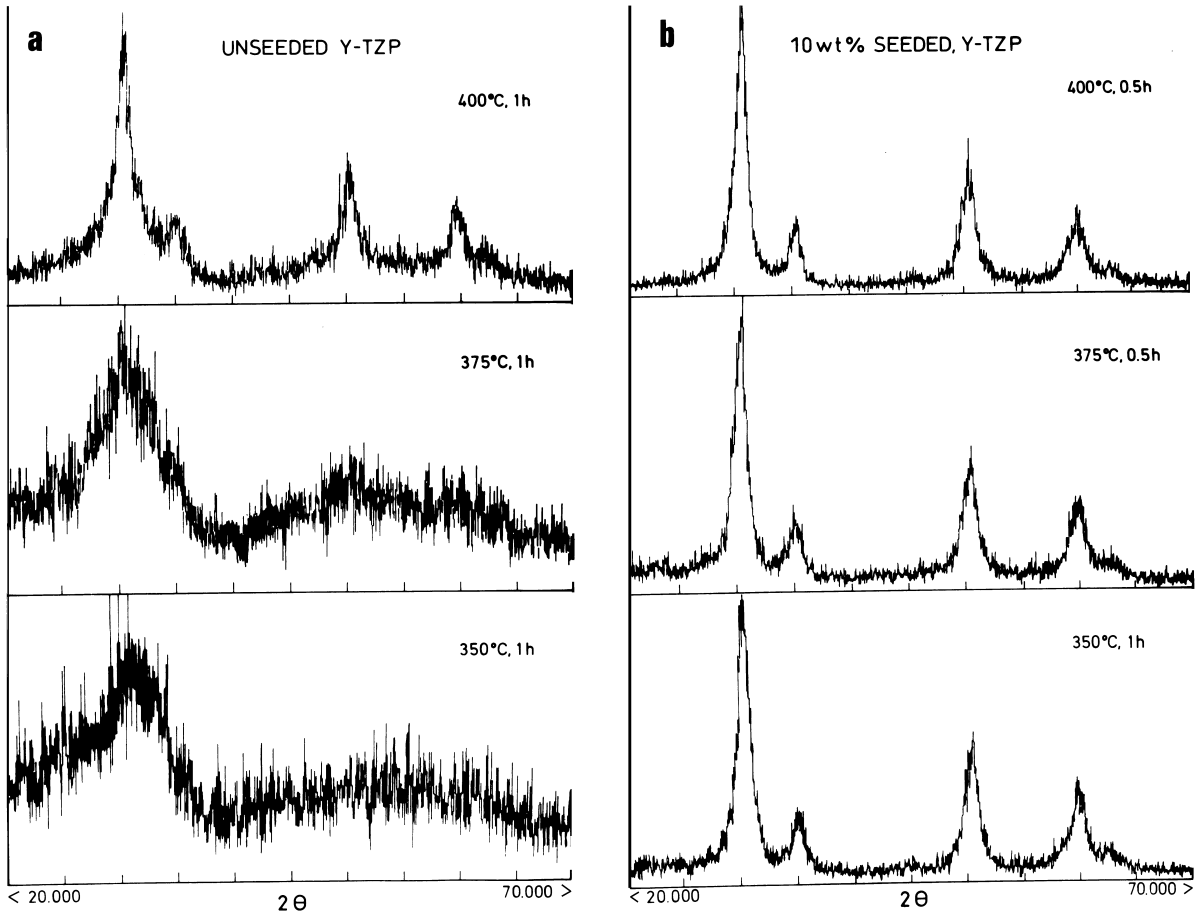

Fig. 3. XRD patterns for (a) unseeded and (b) 10 wt% seeded Y-TZP amorphous precursors, heat-treated at various steps as indicated.

transformations with nanosized seed particles [31–33]. Then, it can be assumed that the epitaxial Y-TZP seeds accelerated the amount of crystalline Y-TZP formed in seeded Y-TZP amorphous precursors, by providing a great number of nuclei with the same structure of the final Y-TZP phase. A similar epitaxial crystallisation was observed in rutile-seeded titania gels (0.2% of rutile seeds). The transformation gel to rutile occurred at a temperature near 250°C lower than the unseeded TiO_2 gel [32].

3.2. Crystallisation kinetics

It has been suggested that the crystallisation of pure tetragonal zirconia could be considered as a nucleation and growth process [28,34], then plotting, as an example, the fraction of crystallised Y-TZP phase as a function of log time, curves of the sigmoidal shape should be obtained in close agreement with de Avrami model [35], which assumes that growth is controlled by nucleation. Fig. 4 shows such a plotting for unseeded and seeded Y-TZP amorphous precursors at 350°C. The curves have almost the same shape and slope which indicates that seeding does not influences the crystallisation mechanism but only the crystallisation rate. As it can be observed the influence of seeding on the crystallisation rate of Y-TZP is so high that the seeded crystallisation almost reaches completion as the unseeded crystallisation begins.

From the above results it seems evident that the kinetics of the Y-TZP crystallisation were reasonably enhanced by seeding Y-TZP amorphous precursors with polycrystalline Y-TZP nanometer-size particles. As established by the Avrami-type nucleation and growth kinetics, an induction time in which no crystallisation was detected seems to exist. In our case such an induction time was obtained by extrapolation of the linear part of the sigmoidal crystallisation curves to 0% of the formed Y-TZP phase. Thus, as it can be observed, the induction time for the seeded Y-TZP crystallisation was reduced about one order of magnitude by comparison to the unseeded Y-TZP amorphous powders at the same temperature. On the other hand, the total time required for complete crystallisation of seeded Y-TZP was as short as 120 min at 400°C, while not less than 1200 min were necessaries in the case of the unseeded Y-TZP precursors.

According to the above assumption, the Avrami transformation kinetic expression was used to evaluate

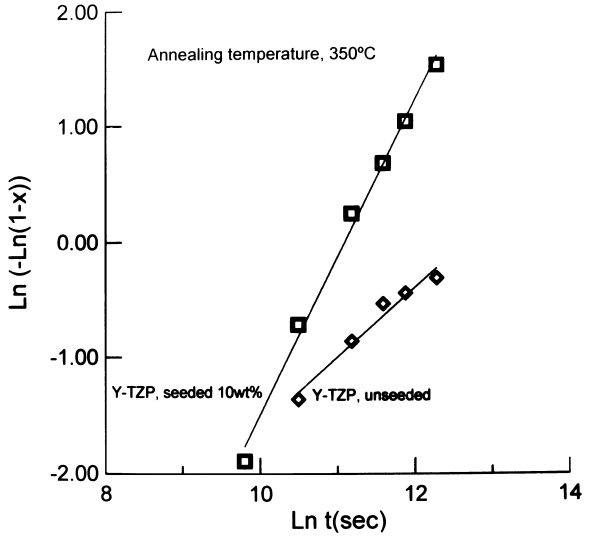

Fig. 4. Avrami plots for the Y-TZP crystallisation at 350°C as a function of the Y-TZP seed concentration.

the XRD data. The relationship between volume fraction and time is given by:

$$x = 1\exp(-kt^n) \quad (1)$$

where n is a constant dependent on the nucleation and growth mechanisms, and k is the rate constant. For isothermal conditions, the experimental data were better fitted according to the following linear transformation of the above equation:

$$\ln[-\ln(1-x)] = \ln\ k + n\ \ln\ t \quad (2)$$

where x is the weight fraction of crystallised Y-TZP phase. Plots of $\ln[-\ln(1-x)]$ as a function of $\ln\ t$ yields the values of n and k. The rate constants, shown in Table 1, were determined from the intercept at each isothermal temperature. As is shown, comparable rate constants were measured at temperatures, at least, 60°C, lower in seeded Y-TZP relative to unseeded samples.

The temperature dependence of k in Eq. (1) apparently follows an Arrhenius relationship, according to:

$$k = A\exp(-E_a/RT) \quad (3)$$

where A is the frequency factor, E_a the apparent activation energy of crystallisation, and R the gas constant. Plots of $\log k$ *vs* $1/T$, as shown in Fig. 5, yielded straight lines with very good correlation coefficients ($\geq$ 0.99). The activation energies calculated were 184 ± 9.2 KJ mol^{-1} and 119 ± 6 kJ mol^{-1} for the unseeded and seeded Y-TZP amorphous precursors, respectively. The activation energy of crystallisation obtained in the case of the seeded Y-TZP amorphous precursors is much lower than that reported for the crystallisation of doped hydrous zirconia (4 mol% Y_2O_3), 262 kJ mol^{-1} [36].

Table 1
Kinetic constant k, and activation energy, E_a, for the crystallisation of unseeded and 10 wt% seeded Y-TZP amorphous precursors

Temperature (K)	k(sec^{-1}) SAMPLES	
	Y-TZP, unseeded	Y-TZP,seeded 10wt%
593	–	3.20×10^{-5}
623	7.21×10^{-6}	5.75×10^{-5}
648	3.20×10^{-5}	–
673	9.98×10^{-5}	5.88×10^{-4}
E_a(kJ/mol)	184 ± 9.2	119 ± 6.0

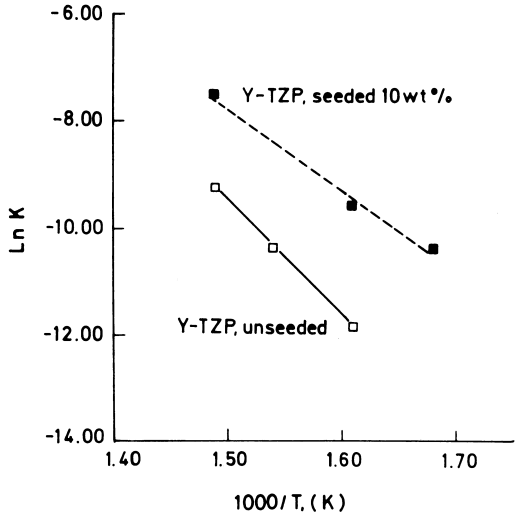

Fig. 5. Arrhenius plots of crystallization rate constant for air-calcined unseeded and 10 wt% seeded Y-TZP amorphous precursors.

These results supported the statement that the presence of nanometer-size Y-TZP seed particles lowered the activation energy to reach the critical nuclei size and, thus, the activation energy for the crystallisation process of the seeded Y-TZP amorphous precursors.

3.3. Calcined powder characterisation

In order to produce completely transformed Y-TZP powders, the seeded Y-TZP coprecipitated amorphous precursors were calcined at 375°C for 10 h (in the following SACC-375), attrition milled for 2 h in pure 2-propanol with zirconia ball media, and dried at 80°C overnight. Typical TEM micrograph of the as calcined powders is shown in Fig. 6(a). It can be noted that the morphology of the SACC-375 powder consisted of relatively agglomerated rounded crystallites with a uniform size distribution. Because of the low calcination temperature point contacts was the predominant bonding between particles. From the TEM micrographs a particle size of about 10 nm could be measured. Fig. 6(b) shows the electronic diffraction pattern of the

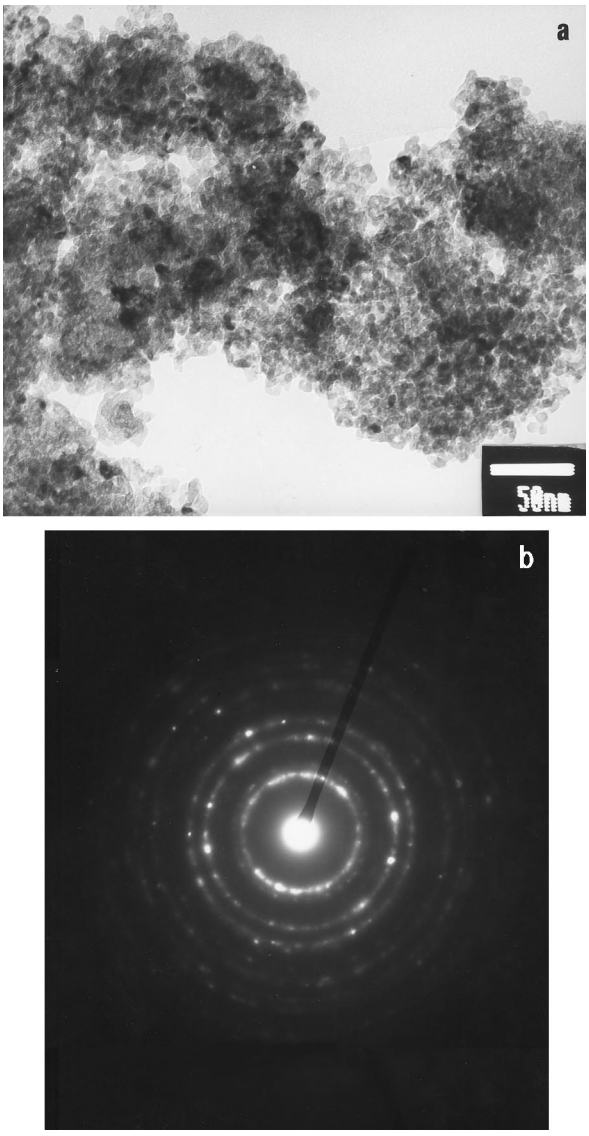

Fig. 6. TEM micrograph of (a) SACC-375 powders and (b) electronic diffraction pattern.

SACC-375 powder. The specific surface (BET) was $114\,m^2\,g^{-1}$ and the crystallite size as measured by XRD was of 14 nm.

Fig. 7(a) shows the adsorption-desorption isotherm curves and Fig. 7(b) the pore size distributions for SACC-375 powders. The isotherm curve is representative of a well-developed mesopore structure, but when compared with that of Fig. 7(b) it can be observed the presence of a certain amount of micropores (<1 nm). Even so, these results confirm the TEM observations of almost spheroidal particles with a relatively low agglomeration degree and uniform size. In the following, a commercial tetragonal zirconia powder (Tosoh) formed by spherical agglomerates ($>20\,\mu m$ in size) with primary particle size of 34 nm, and specific surface area (S_{BET}) of 21 $m^2\,g^{-1}$ will be taken as a reference. Figs. 8(a) and (b) show the SEM micrographs of both

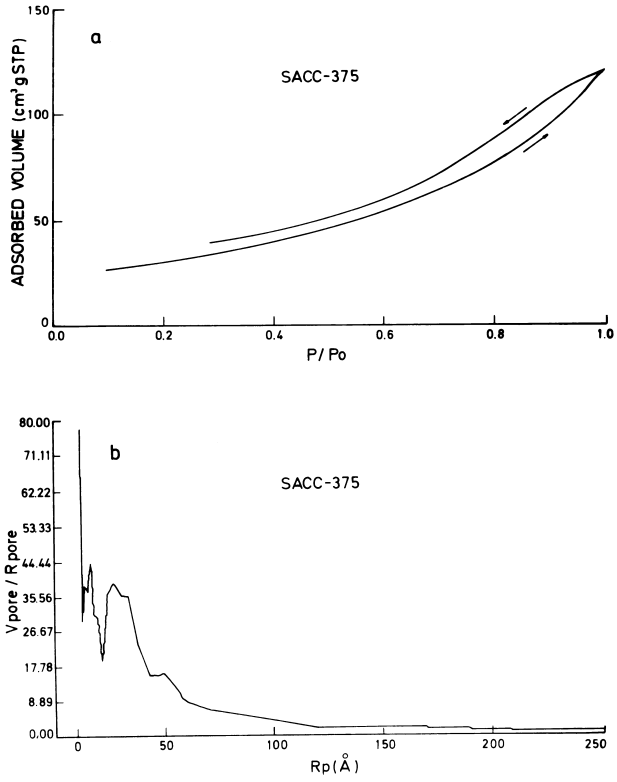

Fig. 7. (a) Adsorption–desorption isotherm curves and (b) pore size distributions for SACC-375 powders.

SACC-375 and Tosoh powders. As it can be observed the SACC-375 powder is a loose one formed by soft agglomerates of about 100 nm in size, which is much smaller than the Tosoh ones.

After compaction at 200 MPa it was found a green density of 45 and 52% of the theoretical density for SACC-375 and Tosoh samples, respectively. From compacts isopressed in the pressure range of 20 to 350 MPa and their relative densities, values of the agglomerates strength of 34 and 40 MPa for SACC-375 and Tosoh powders, respectively, were found. SEM microstructures observations of green compacts showed the presence of sharp edges density inhomogeneities in both kind of samples. Fig. 9 shows the pore size distributions in green compacts after isopressing at 200 MPa. The average pore size diameter were of 14 and 37 nm for the SACC-375 and Tosoh samples, respectively. Although the Tosoh sample has a higher average pore diameter but its pore size distribution is narrower than that of the SACC-375 samples. This has a wider pore size distribution with pore sizes between less than 3 and 40 nm in diameter, and although the presence of a second peak in the pore size distribution curve is not clear but a shoulder towards the smaller pore sizes is detectable, indicating a certain agglomeration degree in the SACC-375 green compacts. This compaction behaviour is in excellent agreement with the microporous–mesoporous structure of the SACC-375 calcined powder.

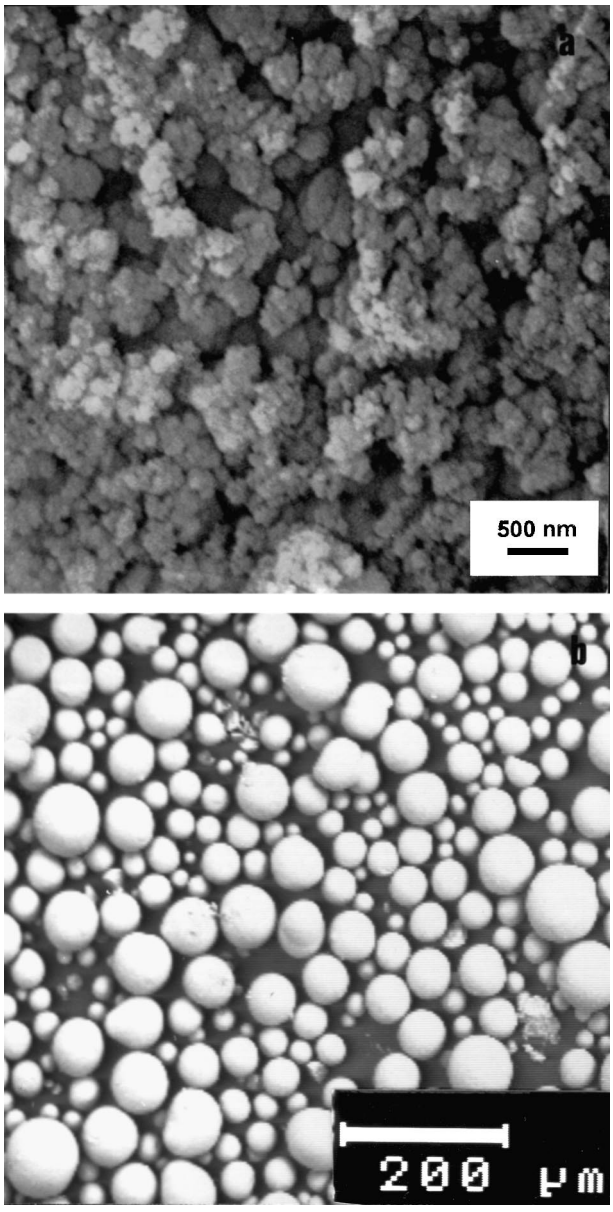

Fig. 8. SEM micrographs for (a) SACC-375 powders and (b) as received Tosoh powders.

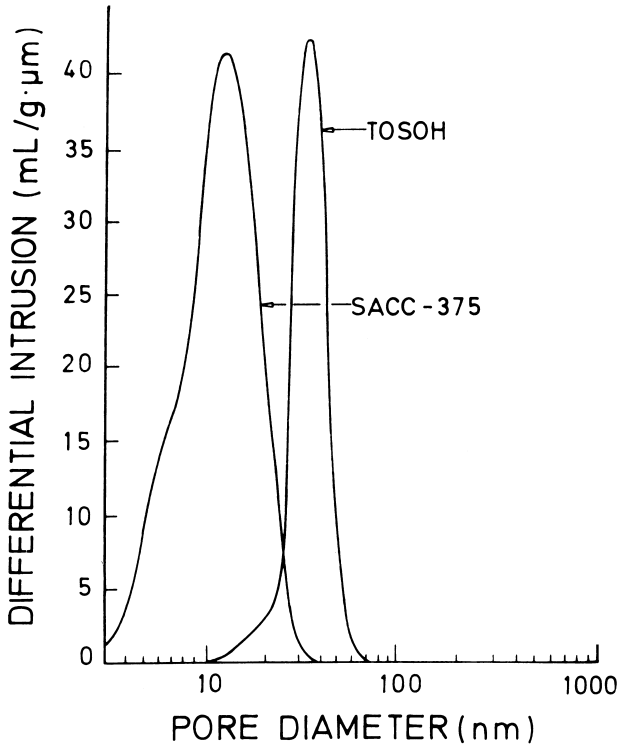

Fig. 9. Pore size distributions in SACC-375 and Tosoh green compacts.

3.4. Sintering behaviour

From the above data and taking into account the specific surface area and the particle size of the two kind of tetragonal zirconia powders, it could be predicted that densification during sintering will proceed at lower temperatures and with higher rates in the case of the SACC-375 green compacts, because of the greater surface area to volume ratio. Fig. 10 shows the shrinkage behaviour of the two tetragonal zirconia green compacts. As expected, densification of SACC-375 sample starts at a temperature as low as 600°C, which is much lower than that of the commercial sample (1000°C). As stated elsewhere [37] at this sintering stage the smaller pores, i.e., intercrystallite porosity, are eliminated. Such intercrystallite porosity is much higher in the SACC-375 samples, and for this reason the densification starting of the commercial sample is delayed up to about 1100°C. An end point density was present in the two samples but a lower shrinkage was produced in the commercial one.

Sintering behaviour of the two kind of samples as a function of the temperature is shown in Fig. 11 The samples were held at each temperature for 5 h with 5°C min^{-1} heating and cooling rates. In the case of the SACC-375 samples a markedly enhanced sintering was observed during the early stages of sintering (below 900°C). Such a behaviour can be explained as the consequence of a higher amount of intercrystallite porosity present in the SACC-375 green compacts which is rapidly eliminated and, thus, at 900°C the density was as high as 92% of theoretical. At 1050°C the samples reached near theoretical density (≥99%), but between 1100°C and 1200°C an abnormal sintering behaviour was observed for the SACC-375 samples, and low densities (≤95%) were achieved. Above 1200°C and up to 1400°C newly a high density (∼99%) was achieved, but it does not reach theoretical value with increasing temperature. Although several causes can contribute to such abnormal densification [38,39], Fig. 12 clearly explains that differential shrinkage, coming from fluctuations in the green compacts density, can be the main source for the lower densification. A similar phenomenon

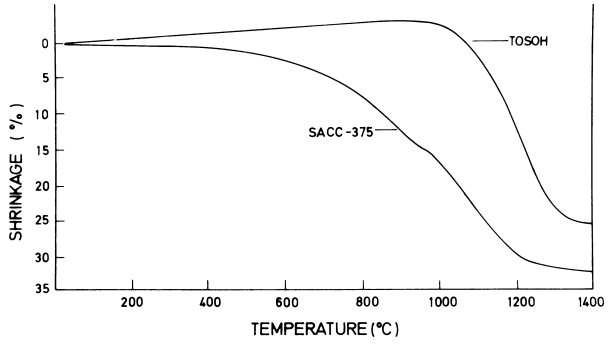

Fig. 10. Shrinkage behaviour of SACC-375 and Tosoh green compacts on sintering.

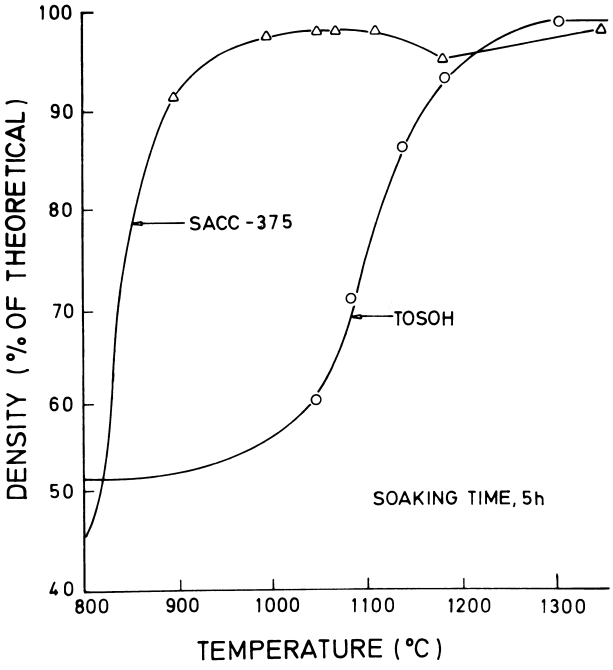

Fig. 11. Sintering behaviour of SACC-375 and Tosoh compacts as a function of the temperature.

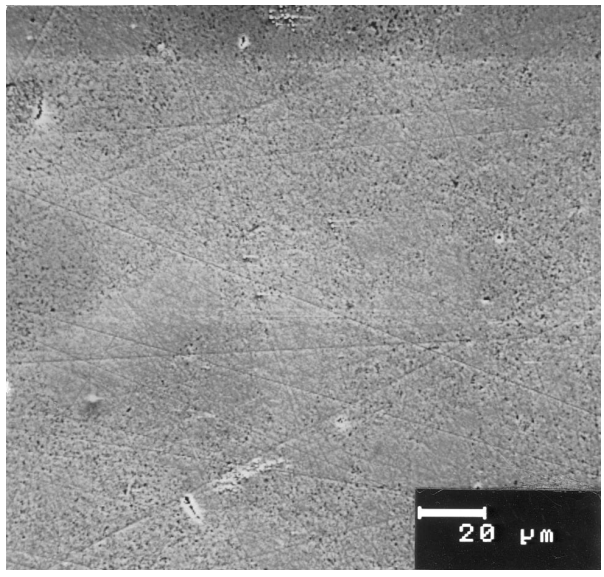

Fig. 12. SEM micrograph of a SACC-375 low-temperature sintered compact showing differential shrinkage.

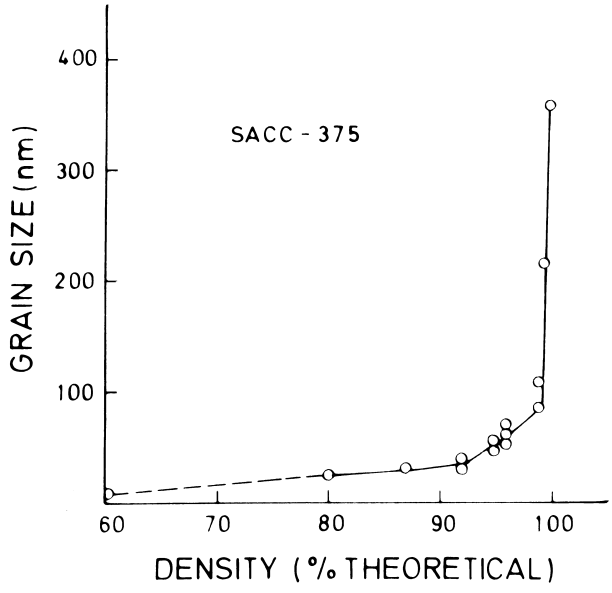

Fig. 13. Grain growth process in SACC-375 sintered compacts as a function of the sintering density.

was found by Chen and Mayo [7] during the sintering of a ultrafine Y-TZP powder. For commercial samples, density monotonically increases with increasing temperature reaching near full density (>99%) at about 1300°C (250°C higher than for the SACC-375 sample). No abnormal densification was detected for the Tosoh samples.

From the above results it seems clear that (a) the small particle size in the SACC-375 powders accelerated the densification kinetics at the early sintering stages leading to almost fully dense bodies at low temperature, (b) the presence of large agglomerates with relatively small pores and with a uniform pore size distribution in the green compacts, as it is the case of the commercial powder, displaces the achievement of full density at higher temperatures and (c) the existence of a quasi bimodal pore size distribution in the SACC-375 powder with many small pores but some of them greater than 40 nm, can be detrimental to achieve fully densified bodies.

As above mentioned, a final density of 99% of theoretical is achieved beyond 1200°C for the SACC-375 samples, which is indicating that a residual porosity can not be eliminated from the structure. As it was shown in Fig. 12 spherical shaped defects can be observed with a size of about 2 µm. Most of them are located in zones which separates regions of different densities. These defects were probably formed during compaction and remained after sintering. The apparently abnormal sintering behaviour of this powder above 1100°C could be

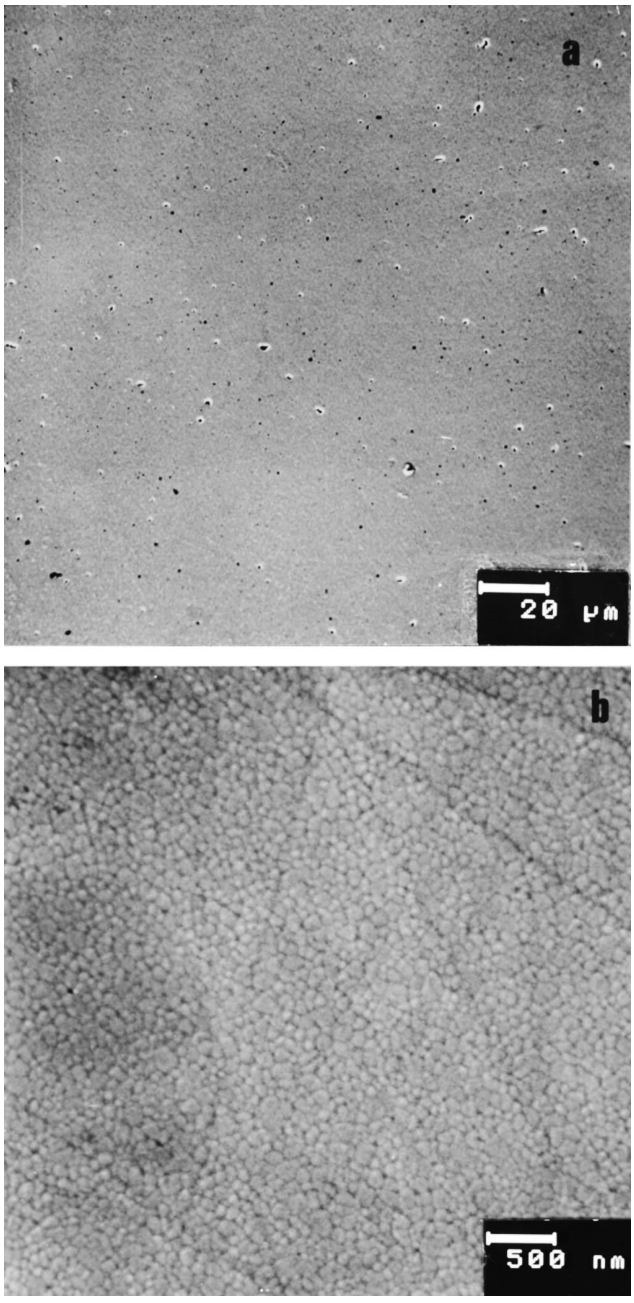

Fig. 14. SEM micrographs of (a) unetched surface and (b) thermally etched polished surface of a SACC-375 compact sintered at 1050°C for 5 h.

interpreted taking into account the critical pore-size to grain-size ratio postulated by Kingery et al. [38,39] Thus the densification behaviour of SACC-375 compacts below 1100°C could be justified because of the majority of the pores are very small respect to the grain size and, therefore, the pore-size to grain-size ratio is below the above postulated critical one. At about 1100°C, a certain pore coalescence takes place and the pore size is higher than the critical ratio, then the density decreases. Parallelly a slow grain size increasing is occurring. Above 1200°C, a substantial grain growth takes place and newly the pore size is below the critical ratio, they shrink and the density increases. As it is shown in Fig. 13, the grain size slowly increases up to a density value of about 92% of theoretical, i.e., when the predominant porosity is practically due to the open pores. Above that density the grain growth rate is accelerated and suddenly increases when the porosity is near to zero. These results indicate that below 92% of theoretical density the open pores act like pinning grain boundaries and the grain hardly grew [39]. This phenomenon takes place in the earlier densification stages. As the open pores are closed the grain growth proceeds at a relatively high rate, and when they have almost disappeared the grain growth rate fastly increased. These different steps for the grain growth process correspond to the densification stages well established for nano-crystalline Y-TZP sintering elsewhere [40,41]. Fig. 14. shows the surface of the non-etched and etched SACC-375 samples sintered at 1050°C for 5 h with a quite uniform microstructure.

4. Summary

Yttria-doped tetragonal zirconia (Y-TZP, 3 mol% Y_2O_3) amorphous precursors seeded with 10 wt% nanocrystalline Y-TZP particles were air-crystallised in the temperature range of 320–375°C, which is at least 50 to 100°C lower than the crystallisation temperature of the Y-TZP phase formed in air-calcined unseeded Y-TZP amorphous powders. Furthermore, a strong increase in the crystallisation rate (about one order of magnitude higher) of the Y-TZP formed in air-crystallised seeded Y-TZP amorphous powders, relative to the unseeded Y-TZP ones, could be calculated. The mechanism for which such a process takes place is assumed to be a catalysed nucleation by the seeding of nanocrystalline Y-TZP particles. The seeds, being isostructural with the expected equilibrium phase and, therefore, having a close lattice matching, helps to control the thermodynamics of the reaction of formation of the Y-TZP solid solution. It seems to be that a rapid inter-diffusion of the different ions takes place upon the seeds surface which acting as catalysts into the amorphous matrix controlling, thus, the growth process via epitaxial on the introduced nuclei. The isothermal crystallisation process was better fitted by an Avrami-type kinetic relationship for a random nucleation which enhancing the crystallisation rate of Y-TZP, with activation energies of 184 ± 9.2 and $119 \pm 6\,kJ\,mol^{-1}$ for unseeded and 10 wt% seeded Y-TZP amorphous powders, respectively. Since the Avrami model assumes that growth is controlled by diffusion, then the low activation energy found for the Y-TZP crystallisation process would support the contention of surface diffusion as the

dominant mechanism for material transport at this thermal level. Fully transformed seeded Y-TZP coprecipitated amorphous precursors, at 375°C for 10 h in air, retained $>100\,m^2\,g^{-1}$ surface area, compared with $\sim 22\,m^2\,g^{-1}$ for an unseeded commercial Y-TZP powder. The seeded Y-TZP transformed powders exhibited a mainly mesoporous structure with a relatively narrow pore size distribution (average pore radius ~7 nm). Such powder characteristics led to near theoretically dense Y-TZP bodies with a grain size within the nanoscale (< 100 nm), when green compacts were sintered at 1050°C for 5 h.

Acknowledgement

This work was supported by the Spanish Commision of Science and Technology (CICYT) under contract MAT-94-871.

References

[1] R.J. Brook, Advanced ceramic materials: an overview, in: R.J. Brook (Ed.), Concise Encyclopedia of Advanced Ceramic Materials, Pergamon Press, Oxford, 1991, p. 1–8.
[2] G.S.A.M. Theunissen, J.S. Bouma, A.J.A. Winnubst, A.J. Burggraaf, Mechanical properties of ultrafine grained zirconia ceramics, J. Mat. Sci. 27 (1992) 4429–4438.
[3] G.S.A.M. Theunissen, Ph.D. thesis, University of Twente, Enchede, The Netherlands, 1991.
[4] F. Wakai, S. Sakaguchi, Y. Matsuno, Superplasticity of yttria-polycrystals tetragonal polycrystals, Adv. Ceram. Mater. 1 (3) (1986) 259–263.
[5] X. Wu, I.W. Chen, Superplastic bulging of fine-grained zirconia, J. Am. Ceram. Soc. 73 (3) (1990) 746–749.
[6] J. Wittenauer, T.J. Nieh, J. Wadsworth, A first report on superplastic gas-pressure forming of ceramic sheets, Scrip. Metall. Mater. 26 (1992) 551–556.
[7] D.J. Chen, M.J. Mayo, Densification and grain growth of ultrafine 3 mol% Y_2O_3–ZrO_2 ceramics, Nanostructured Mater. 2 (1993) 469–478.
[8] G. Skandan, H. Hahn, B.H. Kear, M. Roddy, W.R. Cannon, The effect of applied stress on densification of nanostructured zirconia during sinter-forging, Mat. Lett. 20 (1994) 305–309.
[9] T.G. Nieh, H.J. Wadswort, Effects of grain size on superplastic behaviour of Y-TZP, Scrip. Metall. Mater. 24 (1990) 763–766.
[10] A.J.A. Winnubst, G.S.A.M. Theunissen, A.J. Burggraaf, Compaction and sintering behaviour of nanocrystalline Y-TZP, in: G. de With, R.A. Terpstra, R. Metselaar (Eds.), Euroceramics, Elsevier Applied Science, London, 1989, pp. 1391–1397.
[11] P. Duran, P. Recio, J.R. Jurado, C. Pascual, C. Moure, Preparation sintering, and properties of translucent erbia-doped tetragonal zirconia, J. Am. Ceram. Soc. 72 (1989) 2088–2093.
[12] E. Tani, M. Yoshimura, S. Somiya, Formation of ultrafine tetragonal zirconia powders under hydrothermal conditions, J. Am. Ceram. Soc. 66 (1) (1983) 11–14.
[13] T. Sato, K. Dosaka, T. Yoshida, A. Okuwaki, K. Tori, Y. Onodera, Sintering of ceria-doped tetragonal zirconia crystallised in organic solvents, water, and air, J. Am. Ceram. Soc. 75 (1992) 552–556.
[14] S. Komarneni, R. Roy, E. Breval, M. Ollinen, Y. Suwa, Hydrothemal route to ultrafine powders utilising single and diphasic gels, Adv. Ceramic. Mater, 1 (1) (1986) 87–92.
[15] R. Birringer, H. Herr, H. Gleiter, Trans. Jap. Inst. Metall. (Supp. 27) (1986) 43.
[16] H. Hann, J.A. Eastman, R.W. Siegel, Processing of nanophase ceramics, in: G.L. Messing, E.R. Tuller, H. Hausner (Eds.), Ceramic Transactions, vol. 1B, Ceramic Powder Science II, The American Ceramic Society, Westerville, OH, 1988, pp. 1115–1118.
[17] H. Gleiter, Nanostructured materials: state of the art and perspectives, Nanostructured Mater. 6 (1995) 3–14.
[18] G. Skandan, H. Hahn, M. Roddy, W.R. Cannon, Ultrafine grained dense monoclinic and tetragonal zirconia, J. Am. Ceram. Soc. 77 (7) (1994) 1706–1710.
[19] E. Borsella, S. Botti, R. Alexandrescu, Nanocomposites ceramic powder production by laser-induced gas-phase reactions, Mater. Sci. and Eng A168 (2) (1993) 179–181.
[20] R.W. Siegel, Synthesis and properties of nanophase materials, Mater. Sci. and Eng. A168 (2) (1993) 189–197.
[21] J.L. McArdle, G.L. Messing, Transformation, microstructure development, and densification in α-Fe_2O_3-sedeed boehmite-derived alumina, J. Am. Ceram. Soc. 76 (1) (1993) 214–222.
[22] G.L. Messing, J.L. McArdle, S.A. Shelleman, The need for controlled heterogeneous nucleation in ceramic processing, Mater. Res. Soc. Symp. 73 (1986) 471–480.
[23] J.L. Hulling, G.L. Messing, Hybrids gels for homoepitactic nucleation of mullite, J. Am. Ceram. Soc. 72 (9) (1989) 1725–1729.
[24] L. Pach, R. Roy, S. Komarneni, Nucleation of alpha alumina in boehmite gel, J. Mater. Res. 5 (2) (1990) 278–285.
[25] J. Tartaj, J.F. Fernandez, C. Moure, P. Duran, Influence of seeding on the crystallisation kinetics of air-calcined Y-TZP gel-derived precursors, Mat. Res. Bull., 32 (11) (1997) 1525–1533.
[26] K.P. Klug, L.E. Alexander, X-ray Diffraction Procedures, John Wiley and Sons, New York, 1974.
[27] M.I. Mendelson, Average grain size in polycrystalline ceramics, J. Am. Ceram. Soc. 52 (1969) 443–446.
[28] J. Livage, K. Doi, C. Mazieres, Nature and thermal evolution of amorphous hydrated zirconium oxides, J. Am. Ceram. Soc. 51 (6) (1968) 349–353.
[29] G.S.A.M. Theunissen, Ph.D. thesis, University of Twente, Enchede, The Netherlands, 1991.
[30] M.M.R. Boutz, R.J.M. Olde Scholtenhuis, A.J.A. Winnubst, A.J. Burggraaf, A hydrothermal route for production of dense, nanostructured Y-TZP, Mater. Res. Bull. 29 (1994) 31–40.
[31] G. Vilmin, S. Komarneni, R. Roy, Crystallisation of $ThSiO_4$ from structurally and/or compositionally diphasic gels, J. Mater. Sci. 2 (1987) 489–493.
[32] R. Roy, Y. Suwa, S. Komarneni, Nucleation and epitaxial growth in diphasic (crystalline + amorphous) gels, in: C.C. Hench, D. Urich (Eds.), Science of Ceramic Chemical Processing, Wiley, New York, 1986, pp. 247–258.
[33] G. Vilmin, S. Komarneni, R. Roy, Lowering crystallisation temperature of zircon by nanoheterogeneous sol–gel processing, J. Mater. Sci. 22 (1987) 3556–3560..
[34] R.P. Denkewicz, K.S. Tenhuisen, J.H. Adair, Hydrothermal crystallisation kinetics of m-ZrO_2 and t-ZrO_2, J. Mater. Res. 5 (5) (1990) 2698–2705.
[35] M. Avrami, Kinetics of phase change J. Chem. Phys. 7 (12) (1939) 1103–1112; 9 (2) (1941) 177–184.
[36] R. Srinivasan, R.V. Muraleedharan, S.K. Roy, P.K.K. Nayar, Dehydration and crystallisation kinetics of zirconia yttria gels, J. Am. Ceram. Soc 78 (2) (1995) 429–432.
[37] A. Roosen, H. Hausner, Sintering kinetics of zirconia powders, in: N. Claussen, M. Ruble, A. Heuer (Eds.), Advances in Ceramics, Vol. 12, Science and Technology of Zirconia II, The American Ceramic Society, Columbus, OH, 1984, pp. 714–726.
[38] W.D. Kingery, B. Francois, Sintering of crystalline oxides, 7. Interactions between grain boundaries and pores, in: G.C. Kuczynski,

N.A. Hooton, G.F. Gibbon (Eds.), Sintering and Related Phenomena, Gordon Breach, New York, 1967, pp. 471–498.
[39] W.D. Kingery, H.K. Bowen, D.R. Uhlmann, Introduction to Ceramics, 2nd ed., Wiley, New York, 1976.
[40] P. Duran, M. Villegas, F. Capel, P. Recio, C. Moure, Low-temperature sintering and microstructural development of nanocrystalline Y-TZP powders, J. Eur. Ceram. Soc. 16 (1996) 945–952.
[41] G.S.A.M. Theunissen, A.J.A. Winnubst, A.J. Burggraaf, Sintering kinetics and microstructure development of nanoscale Y-TZP ceramics, J. Eur. Ceram. Soc. 11 (1993) 315–324.